

## Pulsed-Laser-Induced Microcrystallization and Amorphization of Silicon Thin Films

Seiichiro HIGASHI and Toshiyuki SAMESHIMA<sup>1</sup>

Base Technology Research Center, Seiko Epson Corp., 3-3-5 Owa, Suwa, Nagano 392-8502, Japan

<sup>1</sup>Department of Engineering, Tokyo University of Agriculture and Technology, 2-24-16 Naka-cho, Koganei, Tokyo 184-8588, Japan

(Received September 25, 2000; accepted for publication October 25, 2000)

Pulsed-laser-induced microcrystallization and amorphization of Si thin films were investigated by transient reflectance and conductance measurements. It was clarified experimentally that the complete melting of a Si film and subsequent supercooling induces both microcrystallization and amorphization. In the case of the microcrystallization of a 49.1-nm-thick Si film, nucleation among supercooled liquid Si was observed. The nucleation temperature and resulting nucleation rate under the microcrystallization condition were estimated to be 1047 K and  $1.67 \times 10^{25}$  events/(cm<sup>3</sup>·s), respectively. On the other hand, no significant nucleation was observed in the case of a laser amorphization of 20.7-nm-thick Si film although the film was melted for the relatively long duration of about 80 ns. Extremely fast quench of liquid Si films seems to suppress nucleation and results in solidification in amorphous phase.

**KEYWORDS:** pulsed laser, microcrystallization, amorphization, supercooling, nucleation

### 1. Introduction

Low-temperature-process polycrystalline Si thin-film transistors (poly-Si TFTs) are widely used as active devices on insulator substrates such as glass. Currently, they are successfully applied to liquid-crystal displays (LCDs), organic light-emitting diode (OLED) displays,<sup>1–3</sup> sensing devices,<sup>4</sup> memories<sup>5</sup>) and so on. One of the key technologies for the fabrication of poly-Si TFTs under a limited thermal budget is pulsed-laser-induced crystallization of Si thin films. Pulsed laser irradiation to a Si thin film melts the film within a short period of several nanoseconds, and subsequent rapid cooling induces rapid crystalline growth.<sup>6,7</sup> Owing to the localization and short duration of the heat treatment, pulsed-laser crystallization is an effective low-temperature process that allows the use of low-deformation-point substrates such as glass.

It is well known that the crystalline phase of pulsed-laser-irradiated Si thin films strongly depends on the laser energy density and Si film thickness. By irradiating a pulsed laser to amorphous Si films with a laser energy density beyond the crystallization threshold, the phase transformation to polycrystalline occurs. Further increase in the laser energy density results in the increasing grain size of the poly-Si, and eventually induce microcrystallization beyond another threshold laser energy density.<sup>8</sup> Practically, the optimum laser-irradiation condition for device fabrication is a laser energy density that is slightly below the microcrystallization threshold because the crystalline grain size becomes largest at this point. Once the irradiated energy exceeds the microcrystallization threshold, the grain size becomes very small, and results in a microcrystalline phase. Also, it was reported that laser irradiation to Si films thinner than about 30 nm induce amorphization beyond a certain threshold laser energy density.<sup>8,9</sup> Although the pulsed-laser-induced microcrystallization and amorphization of Si thin films have been reported by several authors, the basic understanding of the phase transformation under these conditions has not been clarified yet. In this paper, we report on the experimental examination of pulsed-laser-induced microcrystallization and amorphization. It is clarified that these two phenomena originated from the same melt condition. The only difference between microcrystallization and amorphization is the

nucleation among supercooled Si film.

### 2. Experiments

In order to observe the fast melt and solidification phenomenon, *in-situ* measurements of the transient reflectance and conductance of Si thin films were performed.<sup>10,11</sup> Since liquid Si has a metallic nature, its reflectivity increases from about 50% (50-nm-thick amorphous Si film) to about 75% (molten Si) and its conductance increases about  $10^{-5}$  S/cm (our amorphous Si) to  $1.39 \times 10^4$  S/cm (molten Si)<sup>12</sup> upon melting. By measuring the transient reflectance and conductance of Si thin films, direct observation of the melt and solidification became possible. In order to confirm the crystalline phase following the laser irradiation, the light doping of phosphorus atoms to Si films was performed on several samples. By carrying out a current-voltage measurement of laser-irradiated lightly doped Si films, the microcrystallization or amorphization is instantly confirmed because of their abrupt change in electrical conductivity under these conditions.<sup>9,13</sup> By combining the *in-situ* measurements and post-laser-irradiation electrical measurements, precise observation of the melt, and solidification and confirmation of the resulting crystalline phase were performed. Transient measurements were performed on both lightly doped and nondoped Si films in order to observe the contribution of dopants to the melt and solidification dynamics. We did not observe a significant difference in the transient reflectance and conductance waveforms between lightly doped and nondoped Si films. Therefore, the contribution of dopants to the melt and solidification dynamics is considered to be negligible in our experiment. Transmission electron microscopy (TEM) observation of laser microcrystallized and amorphized films was also performed to confirm their crystalline structure in detail.

Amorphous Si films of 20.7 and 49.1 nm thickness were formed on quartz substrates using low-pressure chemical vapor deposition (LPCVD) through the decomposition of Si<sub>2</sub>H<sub>6</sub> gas at 425°C. SiO<sub>2</sub> films of 100 nm thicknesses were formed by electron cyclotron resonance (ECR) plasma-enhanced chemical vapor deposition (PECVD) at 100°C on amorphous Si films. Then, phosphorous atoms were implanted in the amorphous Si films through the SiO<sub>2</sub> layer

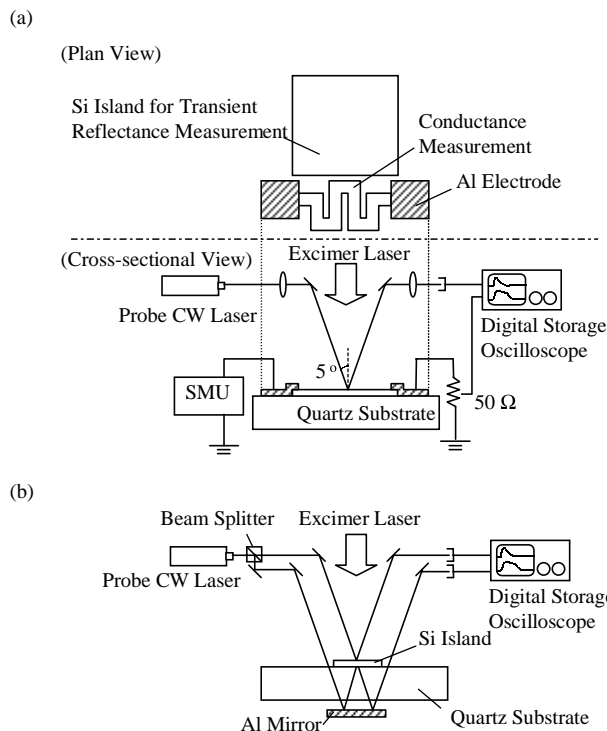


Fig. 1. Experimental apparatus of (a) transient reflectance and conductance measurements of Si films and (b) simultaneous top and bottom transient reflectance measurements of Si films during pulsed laser irradiation.

with the doping concentration of  $5.9 \times 10^{18} \text{ cm}^{-3}$ . After removing the capping  $\text{SiO}_2$  layer, these amorphous Si films were patterned into island-(1 mm  $\times$  1.4 mm) and stripe-shaped ( $L/W = 5000 \mu\text{m}/100 \mu\text{m}$ ) forms as schematically shown in Fig. 1(a) in order to observe the transient reflectance and conductance, respectively. Aluminum electrodes 100 nm thickness were formed by vacuum evaporation in order to bias the Si stripe. These samples were placed in a  $2 \times 10^{-4}$  Pa vacuum chamber and were irradiated by a 28 ns pulsed XeCl excimer laser through a quartz window. Laser irradiation by a 7 mm  $\times$  8 mm shaped beam was initiated from the crystallization threshold energy ( $160 \text{ mJ}/\text{cm}^2$ ) and multiple laser irradiations were carried out. The laser energy density was increased stepwise with increments of  $80 \text{ mJ}/\text{cm}^2$  using a variable attenuator. A CW laser light of 532 nm was directed  $5^\circ$  normal to the Si film and the reflected light intensity was measured using a reverse-biased p-i-n photodiode (transient reflectance measurement). The Si stripe was biased to 20 V by a source measurement unit (SMU: Keithley 236) and the transient current traveling through the molten Si was measured using  $50 \Omega$  load resistance (transient conductance measurement). Along with the measurement of excimer laser pulse intensity using the reverse biased p-i-n photodiode, these transient signals were measured simultaneously by a digital storage oscilloscope (LeCroy 9384CM). After the transient reflectance and conductance measurement during laser irradiation, electrical conductivity of the Si film was measured using the same stripe pattern and the SMU. These measurements were performed at each laser irradiation and repeatedly performed during multiple laser irradiations with increasing laser energy density.

In order to see the difference in melting behavior at the top surface and the bottom interface between Si film and quartz substrate, simultaneous transient reflectance measurements

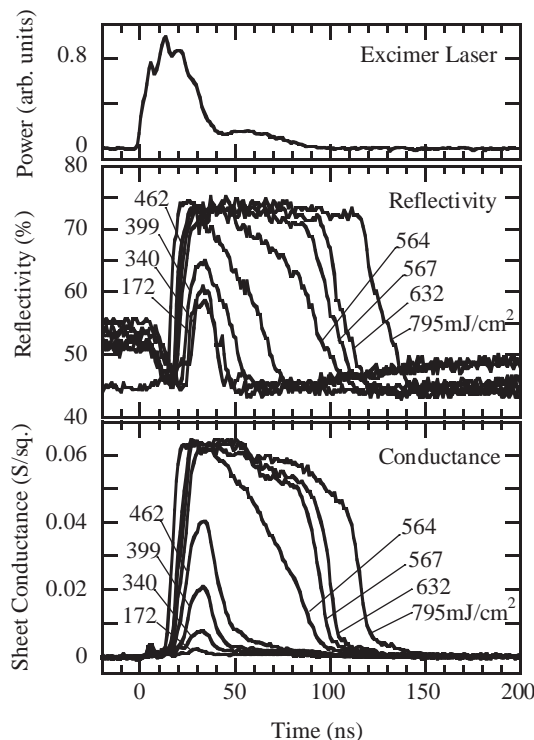


Fig. 2. Observed transient reflectivity and sheet conductance of 49.1-nm-thick Si film as functions of irradiated laser energy density. An example of a pulse waveform of an excimer laser is also shown.

were performed under an experimental setup shown in Fig. 1(b). A probe laser light was split into two beams and one beam was directed to the top surface of a Si film island, while another beam was directed to the bottom interface using an aluminum mirror located beneath the substrate. By measuring the reflected light intensity using two p-i-n photodiodes at the same time, transient reflectance signals of the top surfaces and bottom interfaces were observed simultaneously.

### 3. Results and Discussions

The observed waveforms of transient reflectivity and conductance measurements of 49.1-nm-thick Si films under increasing laser energy density are superimposed in Fig. 2. An example of an excimer laser pulse is also shown and this pulse was used to trigger the oscilloscope. Since the same measurement repeated more than five times exhibited similar results, there was no problem in terms of the repeatability of this measurement. The measured reflectance values were transformed into reflectivity values by calibration measurement using an aluminum mirror under the same measurement conditions. Transient conductance values were transformed to sheet conductance values by considering the aluminum and molten Si contact resistance. Si stripes with three different geometries were used for the transient conductance measurement and the contact resistance was estimated to be  $448 \Omega$ . We feared that the lateral heat diffusion near the aluminum electrodes might affect the local solidification conditions, resulting in the nonuniform solidification of Si films. However, very good linearity was observed among those three different geometry Si stripes; therefore, we could confirm that the observed transient conductance exhibited the transient behavior of a molten Si stripe. As shown in Fig. 2, the melting of Si

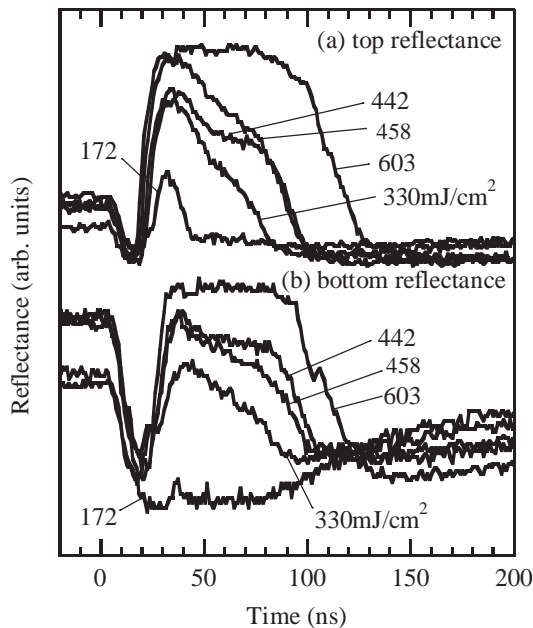


Fig. 3. Observed simultaneous top and bottom reflectance of 49.1-nm-thick Si film during pulsed laser irradiation.

films was observed 20 to 30 ns after the irradiation of the excimer laser, and the melt duration increased with increasing laser energy density. The initial drop in the transient reflectivity waveform is caused by the changing refractive index of the solid Si film with increasing temperature. This was confirmed because the transient reflectivity below the crystallization threshold exhibited identical traces with the initial drop. Increasing the laser energy density increased the maximum molten Si volume, eventually melt the entire film, and this complete melting was marked by saturation of the transient conductance value. In our experiment, the complete melting of a 49.1-nm-thick Si film was observed at the laser energy density above  $560 \text{ mJ/cm}^2$ . The electrical conductivity of molten Si was calculated from the conductance value under the completely melted condition; this was in the range of  $1.26$  to  $1.30 \times 10^4 \text{ S/cm}$ . This value agrees well with the electrical conductivity of the molten Si obtained by static measurement<sup>12)</sup> and supports our observation of the complete melting.

### 3.1 Partially melted conditions

The pulsed-laser-induced melting and solidification of Si thin films have been discussed based on interface-controlled solidification. This is a model that assumes a single liquid-to-solid interface moving into a Si film and returning to the surface with the velocity of 2 to 3 m per second.<sup>14,15)</sup> If this model is correct, the transient reflectance obtained from the top surfaces and bottom interfaces should exhibit different waveforms due to the layered structure which consists of liquid and solid Si. Figure 3 shows the superimposed waveforms observed by the simultaneous top and bottom transient reflectance measurements explained previously. As seen in the figure, the top and bottom transient reflectance exhibited similar waveforms over a wide range of irradiated excimer laser energy except in the low-energy case ( $172 \text{ mJ/cm}^2$ ). Since  $172 \text{ mJ/cm}^2$  was the laser energy density slightly above the crystallization threshold, only a thin layer of the top surface was melted and the reflectance increase was only observed

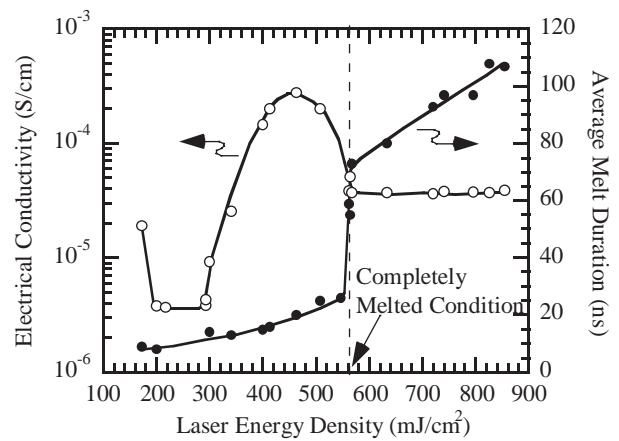


Fig. 4. Electrical conductivity of laser-irradiated 49.1-nm-thick Si film and average melt duration as functions of laser energy density. The Si film was lightly phosphorus doped and the dopant concentration was  $5.9 \times 10^{18} \text{ cm}^{-3}$ .

from the top waveform. Further increases in the laser energy density resulted in similar top and bottom reflectance waveforms; the rising and falling shapes were similar and the melt duration was almost the same. This result can be understood as resulting from the inhomogeneous melting of Si films, which is schematically shown in Fig. 10(b). This result suggests that the melt and solidification of Si films cannot be described by simple interface-controlled growth, but should be described by multidomain and multi-liquid-to-solid interfaces. This may be because multiple laser shots were applied to Si films and there exist inhomogeneous distributions of the disordered structure such as grain boundaries, resulting in nonuniform melting point distributions. The crystalline growth seems to start from these crystalline grains that is not melted and remain in solid phase, which is schematically shown in Fig. 10(c).

### 3.2 Microcrystallization

Figure 4 shows the electrical conductivity and average melt duration of a multiple pulsed-laser-irradiated 49.1-nm-thick Si film as functions of laser energy density. Here, the melt duration was defined by the full width at half maximum (FWHM) of the transient conductance waveform. The electrical conductivity of the laser-irradiated Si film increased with the increasing laser energy density until  $460 \text{ mJ/cm}^2$ , and then started to decrease and finally reached a constant value of about  $3.7 \times 10^{-5} \text{ S/cm}$  beyond  $560 \text{ mJ/cm}^2$ . The decrease in the electrical conductivity of the Si film beyond  $560 \text{ mJ/cm}^2$  indicates the occurrence of microcrystallization.<sup>13)</sup> This was also confirmed by TEM observation which will be discussed later. As shown in Fig. 4, an abrupt increase in the melt duration was observed upon microcrystallization and this sudden increase coincided with the complete melting of the Si film. These results strongly suggest that the complete melting of the Si film [Fig. 10(d)] followed by supercooling induces microcrystallization. Under a supercooling condition, high-density homogeneous nucleation [Fig. 10(e)] is expected; this raises the film temperature to near the melting point, and subsequent nucleation is suppressed. As a result, relatively slow crystalline growth from these nuclei is expected [Fig. 10(f)]. Actually, a slight conductance drop in

completely melted Si film was observed at the time of 57 ns, as shown in Fig. 2, and this can be attributed to homogeneous nucleation. In order to estimate the supercooling, a thermal diffusion calculation was performed. Molten Si film was assumed to be isothermal and no nucleation occurred prior to 57 ns. The molten Si temperature was assumed to be at the melting point at 38 ns because nearly completely melted samples started solidifying at this time. The temporal evolution of the liquid Si temperature  $T_{Si}$  was calculated by a simple one-dimensional thermal diffusion to substrate, which can be described as

$$c_{Si}\rho_{Si}t_{Si}\frac{\partial T_{Si}}{\partial t} = \kappa\frac{\partial T_{Si}}{\partial z}, \quad (1)$$

where  $c_{Si} = 1.04\text{ J}/(\text{g}\cdot\text{K})$  is the specific heat of liquid Si,<sup>16)</sup>  $\rho_{Si} = 2.60\text{ g}/\text{cm}^3$  is the concentration of liquid Si,<sup>17)</sup>  $t_{Si}$  is the thickness of liquid Si,  $\kappa = 0.02\text{ W}/(\text{cm}\cdot\text{K})$  is the thermal conductivity of the quartz substrate,<sup>18)</sup> and  $\partial T_{Si}/\partial z$  is the thermal gradient normal to the liquid Si-to-substrate interface. A linear approximation of the temperature profile in the substrate was applied using the thermal diffusion length and the thermal gradient can be described as

$$\frac{\partial T_{Si}}{\partial z} = \frac{T_{Si} - T_s}{2\sqrt{Dt}} \quad (2)$$

$$D = \frac{\kappa}{c_s\rho_s}, \quad (3)$$

where  $c_s = 1.04\text{ J}/(\text{g}\cdot\text{K})$  and  $\rho_s = 2.2\text{ g}/\text{cm}^3$  is the specific heat and density of the quartz substrate,<sup>12)</sup> respectively and  $D$  is the thermal diffusivity. The temporal evolution of the liquid Si temperature and cooling rate obtained by this calculation are shown in Fig. 5. From this result, the liquid Si temperature at nucleation (57 ns) was estimated to be 1047 K and the cooling rate was estimated to be  $2.16 \times 10^{10}\text{ K/s}$ . This result indicates that supercooling following the complete melting of 49.1-nm-thick Si film comes up to 640 K, which is an extremely strong supercooling, and this value is almost the same as that of the previous report.<sup>19)</sup> The temporal evolution of the nucleation rate was estimated by classical nucleation theory that assumes that the interface energy between liquid and crystalline Si is  $3.4 \times 10^{-5}\text{ J}/\text{cm}^2$ ; the result is shown in the inset of Fig. 5.<sup>20)</sup> The nucleation rate under 640 K supercooling was estimated to be  $1.67 \times 10^{25}\text{ events}/(\text{cm}^3\cdot\text{s})$ . In the case of thin films, the volume of supercooled liquid is limited by the thickness; extremely strong supercooling is required to achieve significant nucleation in this limited volume. In order to confirm the crystalline structure resulting from microcrystallization, observation using high resolution TEM (HR-TEM) was performed. As shown in Fig. 6, almost uniformly distributed microcrystalline grains had an average grain size of 26 nm, and neither a smaller crystalline structure nor an amorphous regime was observed. Cross-sectional TEM observation of microcrystallized Si film was also performed and we observed a random distribution of same-size fine crystalline grains. No preferred crystalline growth either vertical or lateral direction was observed. From these results, the number of grains in a unit area was counted and the nucleation density was obtained. If a single nucleation site originated in each grain, the nucleation density was estimated to be  $3.9 \times 10^{16}\text{ cm}^{-3}$ . Assuming that homogeneous nucleation occurred on a time scale of  $10^{-9}\text{ s}$ ,<sup>20)</sup> the nucleation rate was

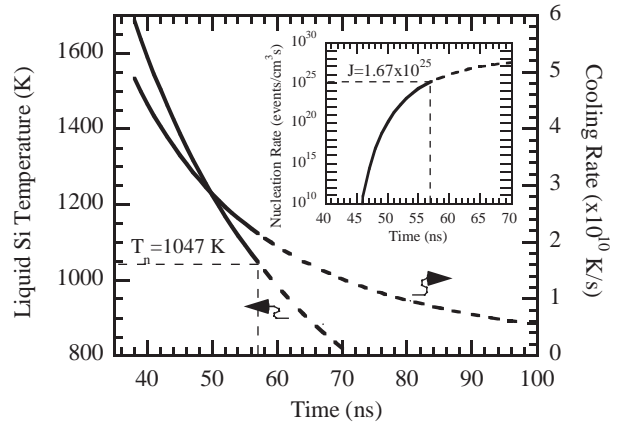


Fig. 5. Calculated temperature evolution of liquid Si film and cooling rate under the supercooling condition. The inset shows the corresponding nucleation rate estimated from classical nucleation theory.

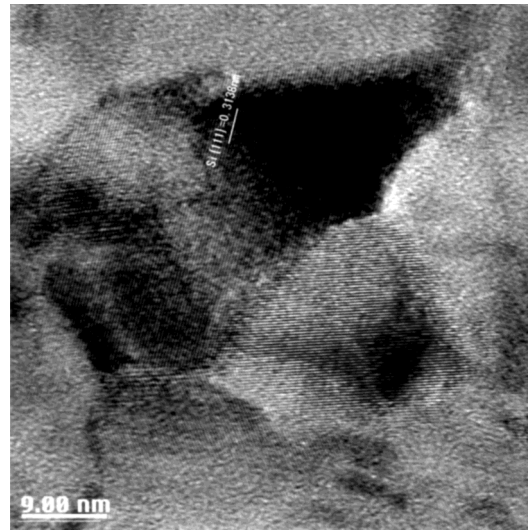


Fig. 6. Plan-view HR-TEM observation image of a 49.1-nm-thick laser-microcrystallized Si film.

estimated to be  $3.9 \times 10^{25}\text{ events}/(\text{cm}^{-3}\cdot\text{s})$ , which agrees in order with the value estimated by the numerical calculation mentioned before. These results suggest that the microcrystallization of a Si thin film is governed by high-density nucleation, which is induced by strong supercooling. Upon nucleation, the temperature of Si film increases rapidly as a result of released latent heat and further nucleation is suppressed. As a result, relatively slow crystalline growth may occur from the nuclei and this slow crystallization is suggested from the transient conductance waveforms, which showed slow decrease following nucleation around 57 ns. Assuming that it took about 53 ns until the completion of crystalline growth from each nucleus, the average crystalline growth velocity was estimated to be 0.25 m/s. This growth velocity is much slower compared to those reported in other studies.<sup>21)</sup>

### 3.3 Amorphization

Pulsed-laser-induced crystallization and amorphization were observed by irradiating an excimer laser on a 20.7-nm-thick Si film. Transient measurements were performed and the measured transient conductance is shown in Fig. 7 along with an example of an excimer laser pulsewave-

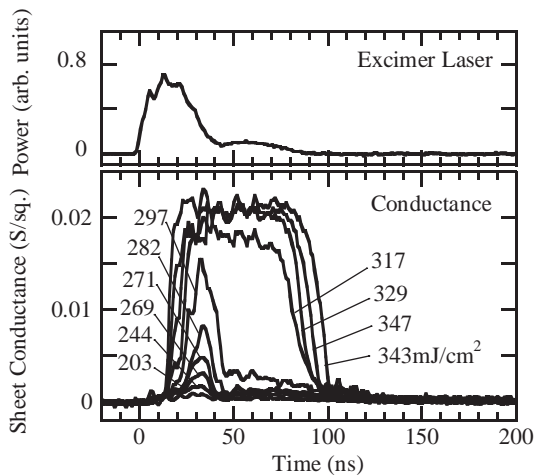


Fig. 7. Observed transient sheet conductance of 20.7 nm Si film as functions of irradiated laser energy density. An example of pulse waveform of excimer laser is shown also.

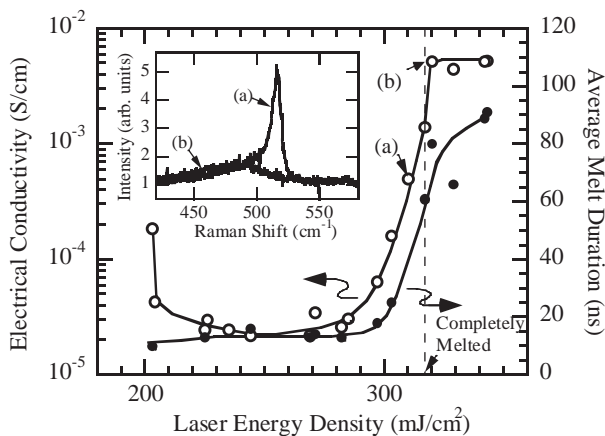


Fig. 8. Electrical conductivity of laser irradiated 20.7-nm-thick Si film and average melt duration as functions of laser energy density. The Si film was lightly phosphorus doped and the dopant concentration was  $5.9 \times 10^{18} \text{ cm}^{-3}$ . The inset shows the Raman TO phonon spectra of Si film under conditions (a) and (b) indicated in the figure.

form. Since the initial reflectivity of 20.7-nm-thick Si film is as high as that of liquid Si film, no significant change in the reflectivity was observed in the transient reflectance waveforms. The electrical conductivity of the laser-irradiated Si film was measured and the result is shown in Fig. 8 along with the average melt duration, which was determined from the transient conductance waveforms shown in Fig. 7. As is evident in the transient conductance waveforms, the melted volume of the Si film increased with increasing laser energy density until complete melting of the film occurred beyond 317 mJ/cm<sup>2</sup> laser irradiation. By melting the entire film, the melt duration abruptly increased to about 80 ns, as shown in Fig. 8. It is interesting to note that the observed transient conductance waveforms are similar to those observed in 49.1-nm-thick Si film. Coinciding with the complete melting, the electrical conductivity of the Si film increased to  $5.2 \times 10^{-3} \text{ S/cm}$  and this value did not change with the increasing laser energy density. In order to confirm the crystalline phase, Raman scattering was performed on those films under the laser-irradiation condition indicated as (a) and (b) in Fig. 8. As shown in the inset of Fig. 8, it was confirmed

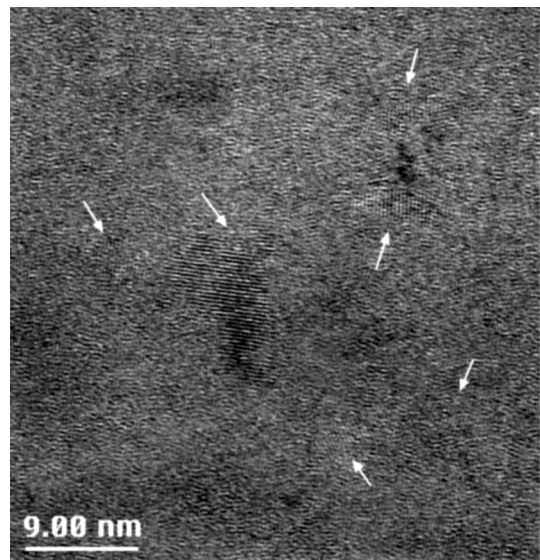


Fig. 9. Plan-view HR-TEM observation image of a 20.7-nm-thick laser-amorphized Si film. Extremely fine crystalline grains, as indicated by arrows, were found in this observation although the majority of the film was completely amorphized.

that the Si film was in the crystalline phase under condition (a) and the amorphous phase under condition (b). This result indicates that the electrical conductivity of laser-amorphized Si film was higher than that of laser-crystallized Si film. This is because the density of midgap defect states are so high in laser-amorphized Si films and carrier transfer in these films is governed by variable-range hopping conduction.<sup>9)</sup> The observed electrical conductivity values of the laser-amorphized films agrees well with those of a previous report studying laser amorphization.<sup>9)</sup> From the above results, it is confirmed that the complete melting of the film induces amorphization [Fig. 10(g)]. This result suggests that both microcrystallization and amorphization are initiated by the same phenomenon, namely, the complete melting of the film and subsequent supercooling. The transient conductance waveforms observed in laser amorphization are similar to those observed in laser microcrystallization except that no significant nucleation sign was observed in the laser-amorphized case. If the 20.7-nm-thick Si film is strongly supercooled, nucleation may occur even in this case. In order to confirm this, plan-view HR-TEM observation was performed. The film was completely amorphized and no crystalline phase was observed. The only exception was that we found a small region containing very fine crystalline grains; this is shown in Fig. 9. In laser-amorphized Si films, these fine grain regions were observed at only two or three points although we searched over an entire 0.3-mm-diameter specimen region and the rest of the film was completely amorphous. These very small grains must be the embryos formed among the strongly supercooled liquid Si. As shown in Fig. 8, laser amorphized Si film was melted for about 80 ns, which is a sufficiently long duration to induce several 100 K supercooling. The grain size of the crystalline embryos (indicated by arrows) was typically 3 to 4 nm. From the separation of each embryo, the nucleation density was estimated to be as high as  $2.2 \times 10^{17} \text{ cm}^{-3}$ , which was higher than that of microcrystallization case. This result suggests the existence of strong supercooling. Unfortunately we

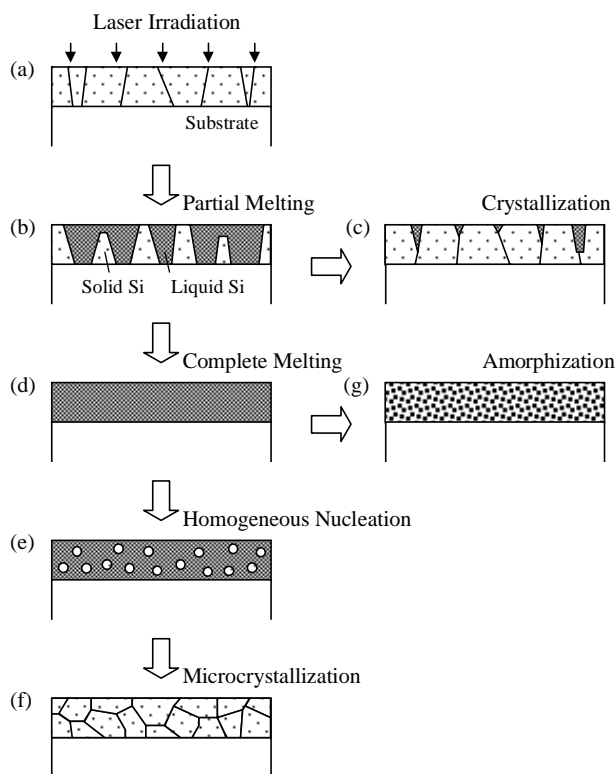


Fig. 10. Schematic diagram of pulsed laser induced melting conditions and resulting crystalline phases. Partial melting of the Si film and subsequent crystalline growth is described by (a), (b) and (c). Complete melting of the Si film results in microcrystallization [(d), (e) and (f)] or amorphization [(d) and (g)], depending on the cooling rate.

have not obtained a definitive answer yet; the nucleation rate may have a peak value under a certain supercooling condition and then be suppressed by further supercooling. In the case of 20.7-nm-thick Si film, the cooling rate is so high that strong supercooling beyond the nucleation peak condition may occur. As a result, Si film is melted for a relatively long duration without significant nucleation and finally solidifies in the amorphous phase. If this is correct, we may observe pulsed laser induced amorphization in thicker Si films, for example, 50 nm thicknesses, if we could increase the cooling rate by some means. This may explain our result, but further examination is required.

Direct amorphous formation from molten Si has been reported using 2.5 ns pulse duration laser irradiation.<sup>22)</sup> This report suggests that a solidification velocity faster than 18 m/s induces direct amorphous formation. However, in our experiment, no such fast solidification was observed. This result indicates that the amorphization induced in Si thin film is not attributable to the fast solidification velocity but is instead attributable to supercooling in the absence of nucleation. Therefore, the amorphization observed in Si thin films originates by a different physical mechanism than that reported previously.

#### 4. Conclusions

Pulsed-laser-induced microcrystallization and amorphization of Si thin films were investigated by transient reflectance and conductance measurements. The melting conditions of

Si films and resulting crystalline phases are schematically summarized in Fig. 10. It was clarified experimentally that the complete melting of a Si film and subsequent supercooling induces both microcrystallization and amorphization. In the case of the microcrystallization of a 49.1-nm-thick Si film, nucleation among supercooled liquid Si was observed. The nucleation temperature and resulting nucleation rate under microcrystallization condition were estimated by numerical calculation to be 1047 K and  $1.67 \times 10^{25}$  events/(cm<sup>3</sup>·s), respectively. On the other hand, no significant nucleation was observed in the case of the laser amorphization of 20.7-nm-thick Si film although the film is melted for the relatively long duration of about 80 ns. Extremely fast quench of liquid Si films seems to suppress nucleation and results in solidification in amorphous phase.

#### Acknowledgements

The authors would like to thank Mr. K. Morozumi of the Material Analysis and Research Center, Seiko Epson Corp. for TEM observation and many suggestions.

- 1) Y. Nakajima, N. Goto, H. Kataoka and T. Maekawa: Dig. Tech. Pap., 2000 IEEE Int. Solid-State Circuits Conf., 2000, p. 188.
- 2) T. Higuchi, J. Hanari, N. Nakamura, K. Mametsuka, M. Watanabe, T. Murai, R. Watanabe, M. Seiki, R. Azuma, Y. Hori, K. Nakamura, Y. Aoki, H. Sakurai, T. Nakazono and N. Harada: Dig. Tech. Pap. 2000 Soc. Inf. Display Int. Symp., 2000, p. 1121.
- 3) M. Kimura, R. Nozawa, H. Maeda, Y. Matsueda, S. Inoue, S. Miyashita, T. Shimoda, H. Ohshima, S. W. B. Tam, P. Migliorato, J. H. Burroughes, C. R. Towns and R. H. Friend: Dig. Tech. Pap., AM-LCD 2000, p. 245.
- 4) N. D. Young, G. Harkin, R. M. Bunn, D. J. McCulloch, R. W. Wilks and A. G. Knapp: IEEE Electron Device Lett. **18** (1997) 19.
- 5) N. D. Young, G. Harkin, R. M. Bunn, D. J. McCulloch and I. D. French: IEEE Trans. Electron Devices **43** (1996) 1930.
- 6) M. O. Thompson, G. J. Galvin, J. W. Mayer, P. S. Peercy, J. M. Poate, D. C. Jacobson, A. G. Cullis and N. G. Chew: Phys. Rev. Lett. **52** (1984) 2360.
- 7) T. Sameshima, M. Hara and S. Usui: Jpn. J. Appl. Phys. **28** (1989) 1789.
- 8) R. Ishihara, W.-C. Yeh, T. Hattori and M. Matsumura: Jpn. J. Appl. Phys. **34** (1995) 1759.
- 9) T. Sameshima and S. Usui: J. Appl. Phys. **70** (1991) 1281.
- 10) G. J. Galvin, M. O. Thompson, J. W. Mayer, R. B. Hammond, N. Paulter and P. S. Peercy: Phys. Rev. Lett. **48** (1982) 33.
- 11) G. J. Galvin, M. O. Thompson, J. W. Mayer, P. S. Peercy, R. B. Hammond and N. Paulter: Phys. Rev. B **27** (1983) 1079.
- 12) H. Sasaki, A. Ikari, K. Terashima and S. Kimura: Jpn. J. Appl. Phys. **34** (1995) 3426.
- 13) S. Higashi, K. Ozaki, K. Sakamoto, Y. Kano and T. Sameshima: Jpn. J. Appl. Phys. **38** (1999) L857.
- 14) M. O. Thompson, G. J. Galvin, J. W. Mayer, P. S. Peercy and R. B. Hammond: Appl. Phys. Lett. **42** (1983) 445.
- 15) M. Hatano, S. Moon, M. Lee, K. Suzuki and C. Grigoropoulos: J. Appl. Phys. **87** (2000) 36.
- 16) P. B. Kantor, O. M. Kisel and E. M. Fomichev: Ukr. Fiz. Zh. **5** (1960) 358.
- 17) A. Ikari, H. Sasaki, E. Tokizaki, K. Terashima and S. Kimura: Jpn. J. Appl. Phys. **34** (1995) L1017.
- 18) S.-M. Lee and D. G. Cahill: J. Appl. Phys. **81** (1997) 2590.
- 19) S. R. Stiffler, M. O. Thompson and P. S. Peercy: Phys. Rev. B **43** (1991) 9851.
- 20) S. R. Stiffler, M. O. Thompson and P. S. Peercy: Phys. Rev. Lett. **60** (1988) 2519.
- 21) J. S. Im and H. J. Kim: Appl. Phys. Lett. **63** (1993) 1969.
- 22) M. O. Thompson, J. W. Mayer, A. G. Cullis, H. C. Webber, N. G. Chew, J. M. Poate and D. C. Jacobson: Phys. Rev. Lett. **50** (1983) 896.